

# JGR Space Physics

## RESEARCH ARTICLE

10.1029/2021JA029894

Z. H. Yao and B. Bonfond contributed equally to this work

### Key Points:

- We quantify two types of auroral intensifications at Jupiter
- During solar wind compression, Jupiter's main aurora was systematically enhanced globally
- During Quiet solar wind conditions, aurora could have either quiet or dawn storm morphologies

### Supporting Information:

Supporting Information may be found in the online version of this article.

### Correspondence to:

Z. H. Yao,  
[z.yao@ucl.ac.uk](mailto:z.yao@ucl.ac.uk)

### Citation:

Yao, Z. H., Bonfond, B., Grodent, D., Chané, E., Dunn, W. R., Kurth, W. S., et al. (2022). On the relation between auroral morphologies and compression conditions of Jupiter's magnetopause: Observations from Juno and the Hubble Space Telescope. *Journal of Geophysical Research: Space Physics*, 127, e2021JA029894. <https://doi.org/10.1029/2021JA029894>

Received 17 AUG 2021

Accepted 12 SEP 2022

### Author Contributions:

**Conceptualization:** Z. H. Yao, B. Bonfond

**Formal analysis:** Z. H. Yao

**Investigation:** Z. H. Yao, E. Chané, W. R. Dunn, W. S. Kurth, J. E. P. Connerney, J. D. Nichols, B. Palmaerts, R. L. Guo, G. B. Hospodarsky, B. H. Mauk, T. Kimura, S. J. Bolton













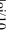
**Methodology:** Z. H. Yao, B. Bonfond, D. Grodent

**Software:** Z. H. Yao, B. Bonfond

**Writing – original draft:** Z. H. Yao, B. Bonfond

**Writing – review & editing:** D. Grodent, E. Chané, W. R. Dunn, W. S. Kurth, J. E. P. Connerney, J. D. Nichols, B. Palmaerts, R. L. Guo, G. B. Hospodarsky, B. H. Mauk, T. Kimura, S. J. Bolton

## On the Relation Between Auroral Morphologies and Compression Conditions of Jupiter's Magnetopause: Observations From Juno and the Hubble Space Telescope

Z. H. Yao<sup>1,2,3</sup> , B. Bonfond<sup>2</sup> , D. Grodent<sup>2</sup>, E. Chané<sup>4</sup> , W. R. Dunn<sup>5</sup> , W. S. Kurth<sup>6</sup> , J. E. P. Connerney<sup>7,8</sup> , J. D. Nichols<sup>9</sup> , B. Palmaerts<sup>2</sup> , R. L. Guo<sup>2</sup> , G. B. Hospodarsky<sup>6</sup> , B. H. Mauk<sup>10</sup> , T. Kimura<sup>11</sup> , and S. J. Bolton<sup>12</sup> 

<sup>1</sup>Key Laboratory of Earth and Planetary Physics, Institute of Geology and Geophysics, Chinese Academy of Sciences, Beijing, China, <sup>2</sup>Laboratoire de Physique Atmosphérique et Planétaire, STAR institute, Université de Liège, Liège, Belgium, <sup>3</sup>College of Earth and Planetary Sciences, University of Chinese Academy of Sciences, Beijing, China, <sup>4</sup>Centre for Mathematical Plasma Astrophysics, KU Leuven, Leuven, Belgium, <sup>5</sup>Mullard Space Science Laboratory, University College London, Dorking, UK, <sup>6</sup>Department of Physics and Astronomy, University of Iowa, Iowa City, IA, USA, <sup>7</sup>Space Research Corporation, Annapolis, MD, USA, <sup>8</sup>NASA Goddard Space Flight Center, Greenbelt, MD, USA, <sup>9</sup>Department of Physics and Astronomy, University of Leicester, Leicester, UK, <sup>10</sup>Applied Physics Laboratory, Johns Hopkins University, Laurel, MD, USA, <sup>11</sup>Frontier Research Institute for Interdisciplinary Sciences, Tohoku University, Sendai, Japan, <sup>12</sup>Southwest Research Institute, San Antonio, TX, USA

**Abstract** Jupiter displays the most powerful auroral emissions in our solar system, which result from strong energy dissipation in Jupiter's surrounding space environment. Although mass and energy in Jupiter's magnetosphere mostly come from the innermost Galilean moon Io's volcanic activity and Jupiter's rotation, solar wind perturbations can play crucial roles in releasing magnetospheric energy. The systematic response of the aurora to a solar wind compression remains poorly understood because of timing uncertainties. Here we report the analysis of a set of auroral images from the Hubble Space Telescope with contemporaneous in situ magnetopause detections from Juno, allowing for a more direct comparison. By analyzing the dawn side main auroral emission, we distinguish two non-mutually exclusive types of auroral enhancements: auroral dawn storm (ADS) featured with latitudinal extension in limited longitudes, and a long-lasting main auroral brightening with limited extension in latitudes while extending over a large longitude range. Only the latter systematically appears under a compressed magnetopause, while the dawn storms could occur whatever the state of the magnetopause. The results could provide important constraints to improve theoretical models and numerical simulations. During expanded magnetopause conditions, Jupiter's aurora displayed either quiet or dawn storm morphology. The result is consistent with recent discovery of the initiation of ADSs in midnight and post-midnight, possibly driven by magnetic reconnection plasma instabilities in night magnetotail. Our results show that some typical auroral morphologies could be used as a diagnostic of solar wind conditions at Jupiter.

**Plain Language Summary** Planetary aurorae are an image of the perturbations of energetic particles in the planetary magnetosphere. Jupiter has the largest magnetosphere in our solar system, and it produces the most powerful auroral emission. Unlike the terrestrial magnetosphere that is mainly driven by solar wind activities, the major plasma source in Jupiter's magnetosphere comes from the innermost Galilean moon Io's volcanic activity. The respective impact of the solar wind and internal plasma sources on Jupiter's magnetosphere and aurorae has been under debate for decades, mostly due to the lack of direct connection between solar wind conditions and auroral morphologies. Using contemporaneous measurements from the Hubble Space Telescope and Juno spacecraft, we can systematically determine the relation between auroral morphologies and magnetopause compression at Jupiter. The results could crucially constrain the physical interpretation of Jupiter's main aurora.

## 1. Introduction

Jupiter has the brightest aurorae of all the planets in our solar system, facilitating the remote observation of energy dissipation across vast distances (Mauk & Bagenal, 2013). The power of auroral components can vary by orders of magnitude in time scales ranging from tens of seconds (Prangé et al., 2004; Waite Jr. et al., 2001) to several

hours (Kimura et al., 2015). The total auroral power is relatively stable, varying by a factor of 2–3 on time scales of hours to days and months, with exceptional transient brightenings by a factor of  $\sim 4$  (Prangé et al., 2001), and can be observed at different wavelengths (Connerney & Satoh, 2000; Dunn et al., 2017; Gladstone et al., 2002; Kurth et al., 1979), indicating comprehensive energy dissipation in the magnetosphere and ionosphere.

In the past three decades, Hubble Space Telescope (HST) has provided high-resolution ultraviolet (UV) images of Jupiter's aurora, which have allowed the identification of several key auroral components, consisting of (a) a main auroral oval, (b) outer emissions essentially formed of injection signatures, (c) a polar region made of a dark region on the dawnside, a chaotic polar swirl region in the center and a polar active region on the dusk flank (Grodent et al., 2003). The main features are well summarized in a review article by Grodent (2015). The main emission is fixed in system-III longitude (i.e., following Jupiter's fast rotation), including several complex structures, such as a narrow arc-like structure, discontinuities and diffuse patches. The main aurora is magnetically mapped to 20–30  $R_J$  ( $1 R_J = 71,492$  km). The outer emissions indicate auroral signatures at lower latitudes than the main emission, corresponding to the magnetospheric processes occurring within 20  $R_J$ , which could sometimes extend to Io orbit ( $\sim 6 R_J$ ). The polar swirl and active regions are highly dynamic, corresponding to outer magnetospheric processes.

Although more and more observations of Jupiter's aurora were obtained by space telescopes and camera onboard orbiters, the mechanisms for Jupiter's auroral components are still far from well understood. The outer auroral injections are, as their name implies, generally agreed to be associated with plasma injection in the middle to inner magnetosphere, thanks to many simultaneous observations from remote sensing telescopes and in situ spacecraft (Haggerty et al., 2019; Mauk et al., 2002; Yao et al., 2020). The polar swirl and active auroral components are poorly understood, as it is challenging to determine which magnetospheric region shall these auroras be connected to. The driver of main auroral oval has been a long-lasting focus in the community and it is widely accepted that the main oval magnetically maps to a distance of 20–30  $R_J$  in the magnetospheric equatorial plane. The leading hypothesis for the formation of Jupiter's main auroral oval is the generation of a magnetosphere-ionosphere coupling current system due to the breakdown of rigid corotation of plasma in the middle magnetosphere (Cowley & Bunce, 2001; Hill, 2001; Southwood & Kivelson, 2001). Notably, because a compression of the magnetosphere would push the plasma inward and increase its angular velocity, this theory predicts that the magnetospheric response to a solar wind would produce a dimmed aurora.

Contrary to these modeling predictions, observations at multiple wavelengths show auroral enhancements during solar wind compressions (Baron et al., 1996; Connerney & Satoh, 2000; Dunn et al., 2016; Echer et al., 2010; Gurnett et al., 2002; Hess et al., 2014; Nichols, Badman, et al., 2017; Nichols et al., 2007, 2009; Sinclair et al., 2019; Zarka & Genova, 1983). Among these observations, the ultraviolet aurora captured by the HST could well inform the exact region of the emission from the main auroral oval, while many other data sets (e.g., radio, X-ray) could not well distinguish the main oval from other components. Nevertheless, these observations still raised serious issues to reconsider the theoretical predictions based on steady-state assumptions (Cowley & Bunce, 2001; Hill, 1979; Southwood & Kivelson, 2001). Two families of explanations were proposed to explain this discrepancy. We shall also note that the main auroral oval is rather well defined and narrow on the dawn-noon side all the time, and during undisturbed times on the dusk side. During disturbed conditions (e.g., compressions), the dusk side main emission (i.e., around or past 18 LT) is highly distorted and bright emissions appear in both higher and lower latitudes. Meanwhile, series of arc structures appear and cannot be easily attributed to the main oval, to outer emissions or to polar emissions.

The first family of solutions are associated with the non-uniform auroral distribution and the multiple auroral components. It is noteworthy that the main emissions, that is, the only part of the aurora to be related to corotation enforcement currents, averagely represents  $\sim 1/3$  of the total power (Grodent, 2015). In time scale of a few hours, the main aurora may dim and brighten, with possible opposite variations of the other components (Grodent et al., 2018). However, spatially resolved observations of the aurora showed that the main emissions were indeed brightening during the solar wind enhancement time intervals (Nichols, Badman, et al., 2017; Nichols et al., 2007, 2009). Another point to consider is the local time variability of the aurora, which was neglected in the first axisymmetric models. Using a local time dependent equatorial magnetic field structure (Vogt et al., 2011) and flux function, Ray et al. (2014) developed a local-time dependent auroral current model, and revealed that the current is strongest in the dawn region from 0500 LT to 0700 LT, surpassing those in the noon through dusk region by an order of magnitude or more. Bonfond et al. (2015) noted that main auroral in the dusk sector was

approximately 3 times brighter than the dawn sector regardless of solar wind conditions, in contradiction with these predictions. Note that transient auroral processes such as dawn storm could lead significant enhanced dawn/morning emission that is much brighter than the afternoon/dusk emission. Vogt et al. (2019) considered the effect of a solar wind-induced compression on the azimuthal component of the magnetic field, on the related radial currents and the resulting aurora as a function of local time, based on Galileo measurements. They concluded that the corotation enforcement currents theory predicts brighter main emissions at dawn and dimmer emissions at dusk during a solar wind compression event.

The second family of explanation for the discrepancy between the initial theoretical expectations and the observations involves the timing of the compression events and the duration of the magnetospheric and auroral response. New interpretations from time-varying modeling (Cowley et al., 2007) and numerical simulations (Chané et al., 2017) have been proposed to mitigate the growing tension between observation and classical steady-state theoretical prediction. Some observational studies relied on the propagation of the solar wind conditions from the Earth's orbit to Jupiter, which are typically affected by a 2-day uncertainty (Nichols et al., 2009; Tao et al., 2005). Some other investigations taking advantage of measurements when spacecraft was arriving at Jupiter (Hess et al., 2014; Nichols, Badman, et al., 2017; Nichols et al., 2007), could reduce the solar wind propagation uncertainty to a few hours. A recent study revealed that solar wind shocks and auroral brightening are coupled by very complicated relations (Kita et al., 2019). Moreover, their study indicated that it requires substantial time (10–15 hr) for Jupiter's aurora to respond to solar wind shock arrival at the dayside front of the magnetopause.

Besides the large scale electrical current system like the current loop associated with the corotation breakdown enhancement force at Jupiter or substorm current wedge at Earth, electromagnetic waves (Alfvén waves) are known to provide substantial contribution to global auroral intensifications (Keiling et al., 2003). Statistical investigations have revealed that Alfvénic precipitation is generally the major source for terrestrial aurora (Newell et al., 2009, 2010), and the field-aligned current may not be the main reason for many regions of the auroral oval (Korth et al., 2014). Theoretical and observations studies have also confirmed the important roles of Alfvénic fluctuation in powering Jupiter's main aurora, outer emission (i.e., equatorward to the main emission) and footprints of the Galilean moons (Damiano et al., 2019; Gershman et al., 2019; Lysak & Song, 2020; Mauk et al., 2017; Pan et al., 2021; Saur et al., 2018). The relative importance between Alfvénic pointing flux and field-aligned currents in driving the main auroral emission (or other auroral components) remains poorly understood.

Juno's first 7 apojoVe periods provided examination of magnetopause compression (Hospodarsky et al., 2017) based on the direct confirmation of magnetopause location in relatively small distance to the planet, which could eliminate uncertainty in solar wind propagation models and could mostly exclude the response time to the solar wind compression at the magnetopause. Meanwhile, HST was used to regularly monitor Jupiter's UV aurora during these orbits. These spatially resolved images allow us to study the brightness of the main emissions for most local times, except the night-side components. Using the comprehensive data sets from Juno and HST, we could perform a systematic determination of the relation between the magnetopause compression and auroral activities with minimal uncertainties on the location and the timing of the response, which is pivotal to assess the proposed interpretations from modeling and simulation investigations.

In this paper, we first carefully examine the morphology of the dawn side main emissions during brightening events and devised a quantitative method to disentangle 2 (non-mutually exclusive) types of morphologies. Then we compare their respective occurrence with the location of the magnetopause deduced from Juno measurements and we found that one was systematically associated with magnetospheric compressions, while the other was relatively independent from them. Aurorae at different local times during compression and quiet solar wind conditions are analyzed. Due to the complexity of the auroral structure in the dusk side, we do not investigate this component in detail in this study.

## 2. Data Sets and the Quantitative Analysis of Auroral Morphologies

### 2.1. Data Sets

In the present study, we analyze Jupiter's UV auroral images from the GO-14634 HST program during Juno's orbit 3–7 (Grodent et al., 2018). These consist of ~40-min long time-tagged exposures in the ~130–182.5 nm range (F25SRF2 filter) from the Space Telescope Imaging Spectrograph (STIS). We use the same procedures to calibrate the images and correct the instrumental effects as in Grodent et al. (2018), including background

subtraction (Bonfond et al., 2012) and conversion from counts to kiloRayleighs (Gustin et al., 2012). Furthermore, we leverage Juno's unrivalled in situ measurements (i.e., Waves (Kurth et al., 2017) and magnetic fields (Connerney et al., 2017)) to examine the conditions of magnetopause compression.

## 2.2. Description of Auroral Morphologies in This Study

Here, we quantitatively analyze the auroral morphologies, to characterize the two types of auroral events, that is, auroral dawn storm (ADS) and main auroral brightening (MAB). The ADS events are often observed on the dawn local times and fixed longitudinally with significant expansions in latitudes (Ballester et al., 1996; Clarke et al., 1998), and the MAB events are auroral brightening on the main arc in all local times within HST's field of view (see an example on 19 March 2017 as reported in Yao et al. (2019)). The dawnside main arc of MAB is usually bright and narrow in the direction perpendicular to the auroral oval, with the discontinuity region near magnetic noon, and afternoon/duskside is bright over a large range of latitudes (Grodent et al., 2018; Nichols et al., 2019). It is noteworthy that the ADS is not necessarily an auroral event developing only on the dawnside. The auroral morphology was captured by HST from the Earth orbit, which could not well cover the nightside auroral component. Recent observations from Juno's Ultraviolet Spectrograph (Juno-UVS) reveal that ADSs are often initiated near midnight and post-midnight, and rotate to dawnside during their developments (Bonfond et al., 2021).

The ADS and MAB events are significantly different for the latitudinal extension and local time variability. For ADS events, the auroral emission is extended to a larger range in latitude, while limited to local times in dawn and morning sectors. In contrast with this, the MAB events are distributed in all local times in HST's field of view, while confined in latitude to a narrow arc in morning local times. The auroral structures in the afternoon/dusk local times during MAB are generally bright while highly complicated. In a recent investigation on the auroral morphologies using large data set (Grodent et al., 2018), six types of auroral events were summarized. ADS and MAB in this study literally correspond to their strong injection and external perturbation families (e.g., family I and X). The quiet auroral morphology is also consistent with the definition in Grodent et al. (2018). In order to characterize the contrasting morphologies of the two kinds of brightening, here we highlight the significant differences in the following two aspects: (a) the MAB's enhanced dawn arc extended to near-noon local times, while the ADS in was limited to the dawn local times before 9 hr; (b) the dawn auroral arc along the reference main oval is thinner and smoother for the MAB, but thicker and more variable along the reference oval for the ADS. We therefore define two parameters that allow us to distinguish between these brightening events: mean arc width of the dawn aurora and the variation of auroral width along the main oval reference, for characterizing the two types of auroral morphologies. The quantitative analysis is provided in the Methods of Section 2.3.

## 2.3. Determination of Mean Auroral Width and Its Standard Deviation of the Dawnside Main Aurora

Here we take two auroral images obtained by HST on 22 and 24 January as two examples to detail the successive steps of our method. Figures 1a and 1d show the weighted sum of the projections onto Jupiter's northern pole of the successive 10-s long auroral images acquired during the whole 40-min long time-tag sequence. Figure 1a is a typical ADS event, as clearly evidenced by the auroral brightening around the dawn arc with significant extension in latitudes. There are four major steps to calculate the mean auroral width and its standard deviation, as described below. For contrast, Figures 1d–1f shows these same steps for 24 January 2017: in this case the aurora is undergoing a clear MAB auroral event. Note that all the auroral images selected in this study are taken from the northern hemisphere. We empirically identify ADS events with mean arc width on the dawn side exceeding 1,400 km and the variation exceeding 500 km, and we identify MAB events with mean arc width on the dawn side below 1,000 km and the variation is below 400 km, based on a limited number of cases. The calculations of mean arc width and its variation are explained below. In this study, the afternoon/dusk auroral emission is not investigated in great detail, as we do not find a consensus on the afternoon/dusk auroral component. It is likely that the complicated afternoon/dusk auroral morphologies are a consequence of multiple mixed processes, for example, plasma injection, wave-particle interaction, dayside magnetodisc reconnection etc., which are probably not highly correlated with solar wind compression. Therefore, we do not discuss the afternoon/dusk auroral emissions in detail in this study.

Since the afternoon/dusk auroral emissions are often highly complex, which often extend to a large range in latitude (see Figure 1d) and sometimes show multiple arcs (e.g., Nichols et al. (2009)). The definition of a main arc

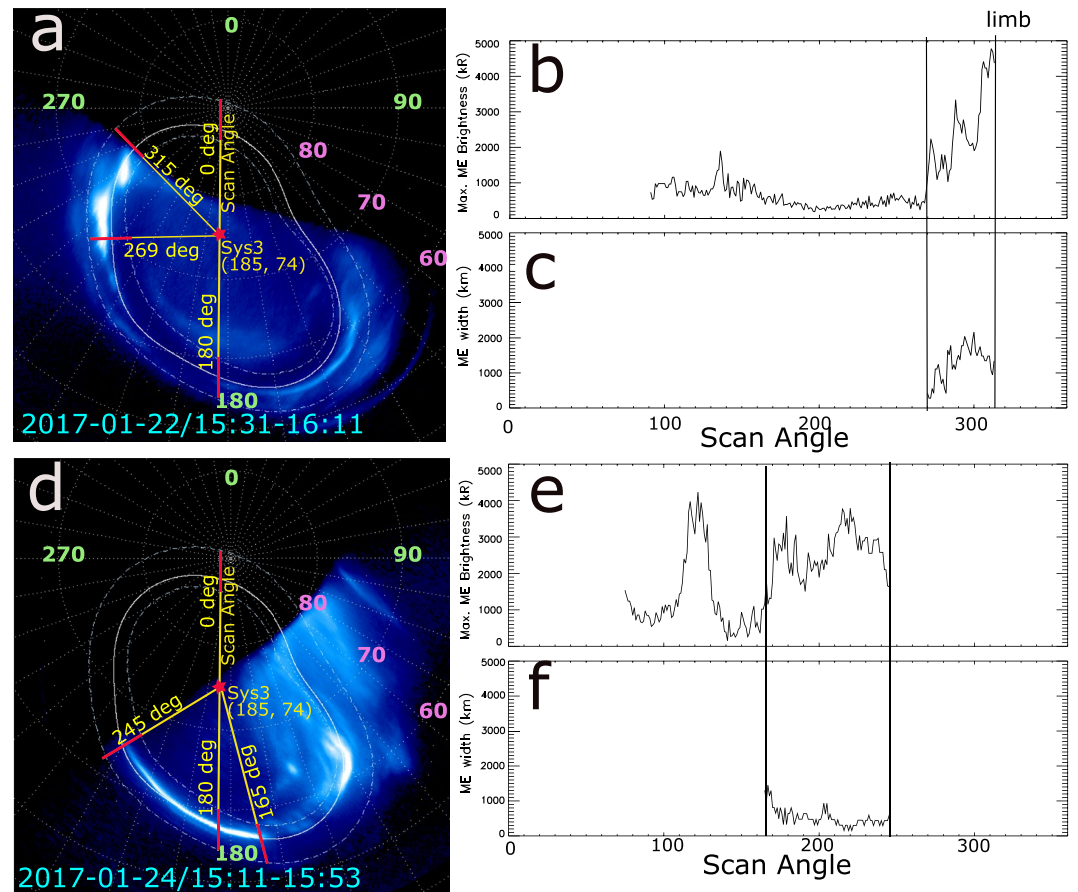


**Figure 1.** Calculation of the main auroral arc width. (a) An auroral example on 22 January 2017. The yellow lines indicate scan angles, and the red star indicates auroral oval's center (System III longitude at 185° and latitude at 74°). (b) Maximum brightness on the main emission along the scan angles. (c) the width of main auroral arc along the scan angles. (d–f) The same format as (a–c) for an auroral image on 24 January 2017. The two events are auroral dawn storm (ADS) (a) and main auroral brightening (MAB) (d) morphologies.

in highly dynamic auroral events could be challenging, especially in the northern hemisphere, as seen from HST with a central meridian longitude around 160°, because the dusk side of the aurora coincides with a magnetic anomaly which distorts and further complicates the morphology. Nevertheless, the brightness distribution along the reference oval of the main emission could still generally represent the local-time variations of main auroral emission. The reference oval of main emission is an average location as described in Bonfond et al. (2012). The complex afternoon/dusk auroral morphology probably indicate a combination of multiple processes, which are to be further investigated.

#### Step 1. Define the scan angle system in polar projection

The auroral image (Figure 1) on the grid (white dotted lines) is in System III coordinates (Fränz & Harper, 2002), which corotates with the planet. The green and pink numbers indicate the System III longitudes and latitudes. The red star denotes the center of main auroral oval (Grodent et al., 2004; Radioti et al., 2008), also known as auroral oval's barycenter (Bonfond et al., 2015). The yellow lines radiating from the auroral barycenter indicate the successive scan angles.

#### Step 2. Identify the auroral maximum brightness along the main oval

We select the maximum brightness along the cut relative to each scan angle in a relatively large area (20 pixels from the reference oval to either inward or outward along the scan direction, each pixel corresponds to ~80 km), whose inner and outer boundaries are marked by the dash dot ovals on the auroral image. As indicated by the red bars in panel (a), the region covers the main auroral emissions well. The maximum brightness as a function of scan angle is shown in panel (b). The total auroral power is the sum of the power of the whole northern hemisphere. The power calculation and correction are shown in Grodent et al. (2018).

Step 3. Calculate the width of the main emission  $\sim$ perpendicular to the auroral oval for each scan angle. The width of main emission in panel c is obtained using the boundary of 50% of maximum brightness for each scan angle. The initial scan angle is determined by intensities  $>1,000$  kiloRayleighs and the final scan angle is determined by the upper limit of scan angle imparted by the viewing geometry in the polar projection. The boundaries are shown in Figure S1 in Supporting Information S1. Since the auroral oval is not circular, it is inevitable that the scan axis is not always normal to the oval and thus would introduce a bias in the calculation of width. The effect is the same to all events, so that the comparison between different events is not affected by this bias.

Step 4. Calculate mean arc width of the dawn aurora and the variation of thickness

As illustrated by the two vertical dashed lines in panels (b and c), we determine the range of scan angle to calculate the mean arc width of the dawn aurora and its standard deviation as the variation of arc thickness. It should be noted that ADS and MAB are not necessarily mutually exclusive. Our analysis focuses on the changing dawn auroral characteristics since afternoon/dusk emissions are difficult to constrain. However, MAB emission, here characterized by narrow dawn emission, are better described as a global enhancement of the aurora - the narrow enhancement highlights the occurrence of a MAB event only if there is not also an ADS event simultaneously occurring. If both occur, the dawn will enhance and broaden under the influence of the ADS event, but other auroral regions will simultaneously brighten. If the two events happen simultaneously, then our method will classify them as ADS. A visual inspection of the main emissions at other local times suffices to identify MAB cases.

### 3. Results

#### 3.1. A Case Study in January 2017: Contemporaneous Measurements From HST and Juno Over 6 Days

To further highlight how our study investigates both auroral morphology and magnetospheric conditions, we first present a case study that highlights how these datasets are compared and contrasted to understand the link between auroral events and their magnetospheric trigger. One of the regular sequences of HST UV imaging observations in coordination with the Juno spacecraft (Grodent et al., 2018) was planned from 22 to 27 January 2017. Figure 2 shows the projections onto Jupiter's northern pole of auroral images integrated over about 40 min. On 22 January, there was an auroral brightening around the dawn arc (Figure 2a), which was not found in the successively available HST image in Figure 2b ( $\sim 29$  hr later). The auroral event on 22 January is a typical ADS as we have introduced in Section 2.2. The auroral image shown in Figure 2c was obtained  $\sim 19$  hr after Figure 2b, which shows a global enhancement in all local times within HST's field of view, and a dawn/morning arc enhancement relatively narrow in width, which is a typical MAB event, as we have previously introduced. If we take the power in Figure 2b (i.e., 1,045 GW) as the baseline of quiet Jovian aurorae, the total auroral power in Figure 2c is enhanced by a factor of two. This auroral morphology remained similar and the power further increased to 2,430 GW in the following HST visit (Figure 2d,  $\sim 1.5$  hr later). The thin enhanced auroral arc on the dawn to noon local times remained in Figure 2e while with significantly decreased power and return to almost quiet time auroral power in Figure 2f. The afternoon/dusk auroral region also show coincident enhancements in Figures 2c and 2d, while distributed in a large range of latitudes (both higher and lower than the main oval) which is quite different to the narrow arc on the dawn side. Therefore, the MAB event likely lasted for about 2–3 days, consistent with previous reports on main auroral enhancements during solar wind compression based on the analysis of observations from HST (Nichols et al., 2007) and Hisaki (Kita et al., 2016). In addition to their typical lifetime, the mean arc width and the variation of the ADS in Figure 2a are 1,468 and 548 km. The two values are 626 km and 262 for the MAB in Figure 2c. The mean arc width and variation in the ADS are a factor of two larger than for the MAB.

A key unsolved question is whether or not the two auroral morphologies correspond to fundamentally different drivers. Disentangling the solar wind influence from other drivers is critical for auroral interpretation. Since the two auroral events were observed 2 days apart, it indicates that a complete transition between the two types of auroral morphologies could be shorter than 2 days. Therefore, it is insufficient to apply a modeling solar wind prediction to assess whether or not the two auroral events happened under different solar wind conditions, since the modeling prediction of solar wind condition usually involves an uncertainty of about 2 days even in ideal conditions (Tao et al., 2005) (e.g., the Earth-Sun-Jupiter angle is less than  $40^\circ$ ). Here we directly identify magnetopause crossings using Juno's Waves instrument (Kurth et al., 2017) and MAG instrument (Connerney et al., 2017) in coordination with HST's auroral context. By comparing with the observation-based magnetopause model by Joy et al. (2002), we can therefore identify intervals when the magnetosphere is compressed based on

Polar projection of HST ultraviolet auroral images (northern pole)

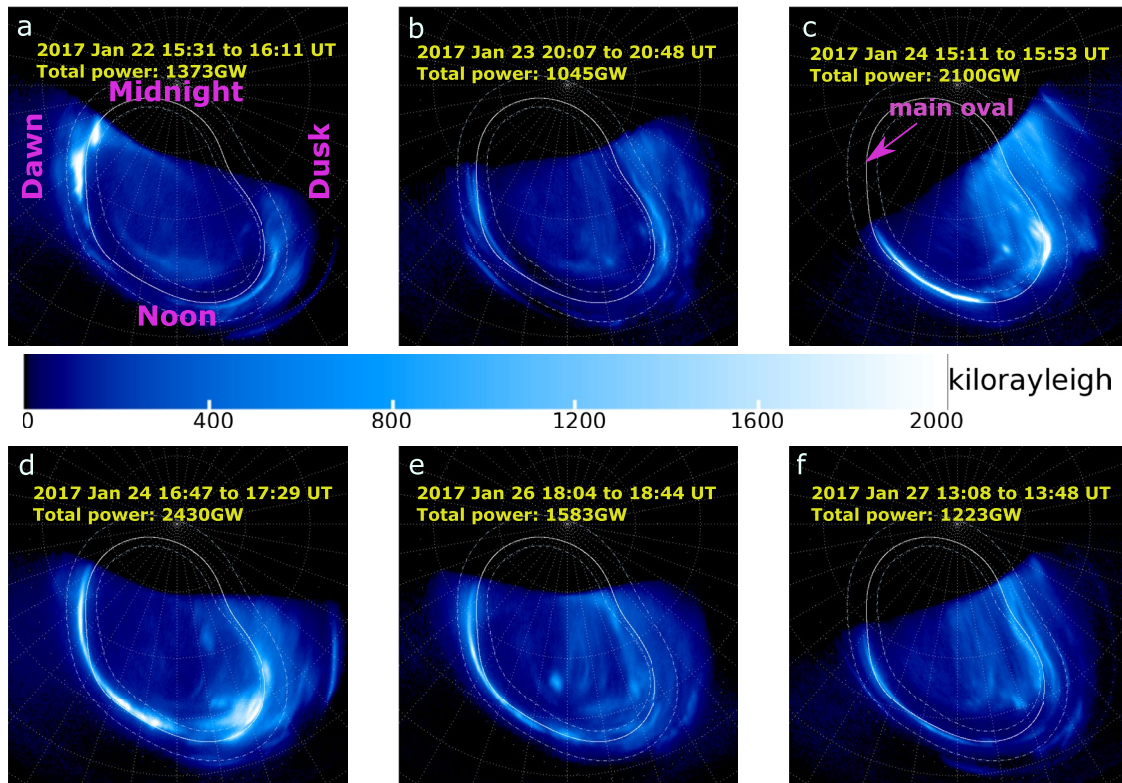


**Figure 2.** Polar projections of six auroral images from 22 to 27 January 2017. Each image was averaged over  $\sim 40$  min. The main oval (indicated by the pink arrow in panel c) is an average main auroral oval location. Figure 2a is a typical auroral dawn storm (ADS) event, and Figures 2c and 2d are typical main auroral brightening (MAB) event.

Juno's in situ observations, so that we accurately assess the influences of solar wind compressions on auroral activities, and provide key information to answer two questions: (a) how does the solar wind modulate Jupiter's main aurora? (b) ADS have previously been observed during solar wind compressions (Kimura et al., 2017; Nichols, Badman, et al., 2017), is there a physical causality or was this coincidence?

Interestingly, the hectometric radio emission with frequency of several MHz (Figure 3a) was enhanced since 24 January when the MAB auroral event was observed, but not significantly enhanced for the ADS event on 22 January. We note that the hectometric emission remained enhanced for at least 2 days after the MAB auroral event (e.g., Figure 2e). Such longer lasting hectometric emission than enhanced aurora has also been detected during Cassini's flyby of Jupiter (Gurnett et al., 2002). The different time durations may be explained by their closely related while different formation mechanisms. Enhanced auroral emissions can only exist when there was an intense electron precipitation. On the other hand, the HOM wave is a consequence of anisotropic electron distributions, among which the loss-cone distributions where electrons are mostly lost into the atmosphere may continually exist when there is no strong precipitation. It requires further theoretical and observational investigations to fully understand this issue.

In the present research, the solar wind conditions are inferred from the location of detected magnetopause. The nominal magnetopause location on the dawnside is at  $>100 R_J$  but it can move to  $\sim 70\text{--}80 R_J$  during strong compressed situations, as suggested by both models (Joy et al., 2002) and Juno's statistical results (Hospodarsky et al., 2017). The basic principle is to compare the standoff distance of the magnetopause with model prediction under nominal and strong compression conditions. There are four possible conditions to be judged: (a) when the magnetopause is detected in relatively inner region (i.e.,  $\sim 90 R_J$ ), we classify the event as compressional event; (b) when the magnetopause is detected in relatively outer region or with unperturbed magnetic fields at  $>85 R_J$ , we identify the event as quiet event; (c) Juno was in relatively outer region and detected the magnetopause, the

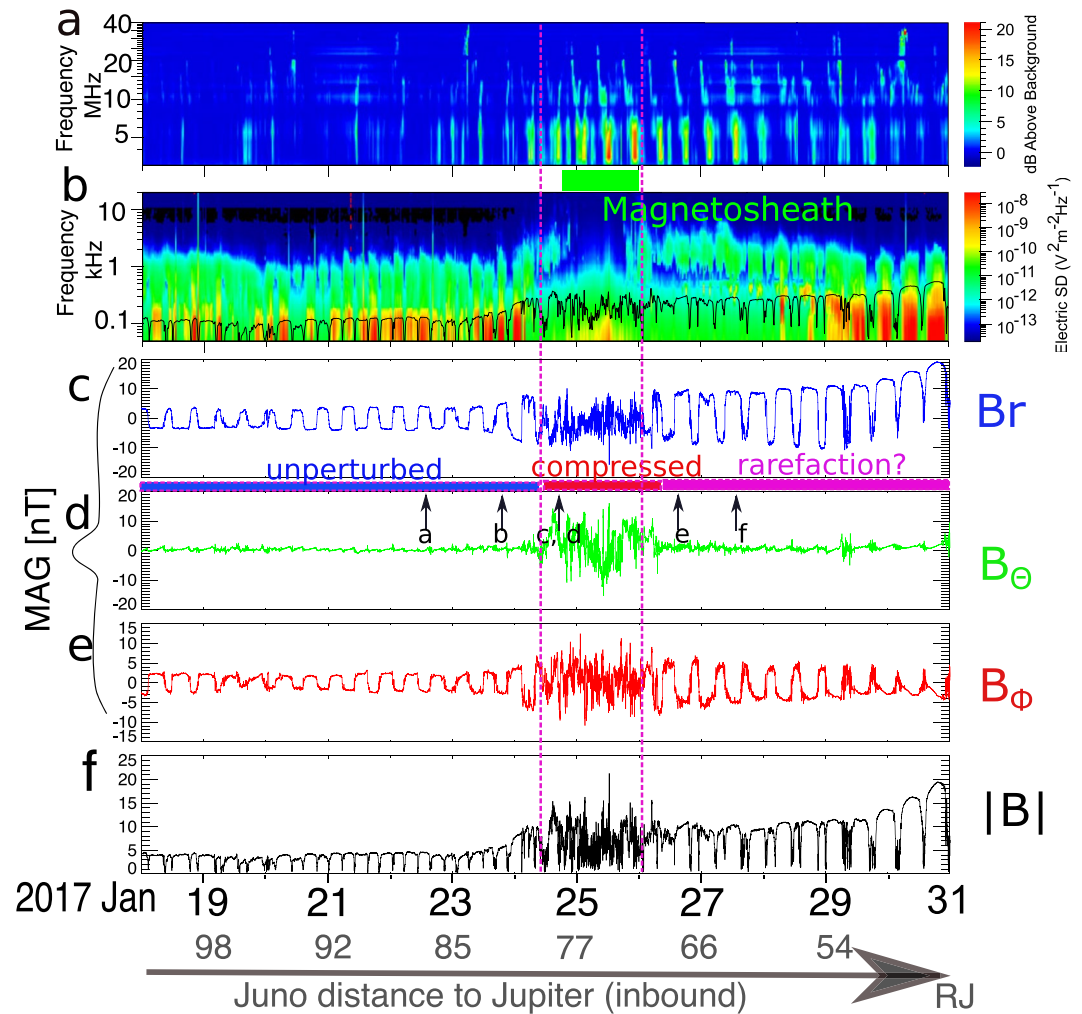


**Figure 3.** Juno's measurements of waves and the component magnetic fields in System III coordinate system, showing unperturbed, strongly compressed and potentially expanding magnetosphere conditions. (a) Plasma wave spectrogram of hectometric and decametric emissions (a few to tens of MHz). (b) Plasma wave spectrogram of electric field from 50 Hz to 10 keV. The disappearance and appearance of  $\sim 1$  kHz continual emission indicate the entry and exit of Juno into the magnetosheath. (c–f) Three components of magnetic fields and the magnetic strength. As marked on the top of panel d, we divide the observations into three periods, that is, unperturbed, compressed and rarefaction conditions. Note that the times for images in Figure 2 are marked with black arrows in panel (d) The electric field wave intensities were computed using the geometric antenna length of 2.4 m.

event is classified as undefined; (d) Juno was in relatively inner region and did not detect the magnetopause, the event is also classified as undefined. Following the above definition, we use the low frequency radio emission to determine the magnetopause crossing in this study. The intense emissions with frequencies between about 200 Hz and 2 kHz (Figure 3b) are the trapped continuum radiation (Gurnett et al., 1980; Scarf et al., 1979), which is usually absent in the magnetosheath. The appearance (or disappearance) of the emission serves as a good indicator of entry into the magnetosphere (or exit into the magnetosheath) for a spacecraft (Gershman et al., 2017; Hospodarsky et al., 2017; Kurth et al., 2002). During ultraviolet auroral observations in Figure 2, Juno traveled inbound from  $>110$  to  $\sim 70 R_J$  to the planet center in the sector (near 05:00 Magnetic Local Time), and encountered an inward moving magnetopause (Figure 4) on 24 January at  $\sim 78 R_J$ , so that Juno was exposed to the magnetosheath thereafter (marked by the green bar on the top of panel (b) in Figure 3). On 26 January Juno returned to the magnetosphere (evidenced by the reappearance of the trapped continuum radiation), which is likely due to the recovery of magnetopause to a more expanded configuration. The strongly perturbed magnetic field between 25 and 26 January also confirms that Juno was in the magnetosheath. The wave frequencies, which reflect the plasma number density (Kurth et al., 2002), has significantly increased shortly before (after the first



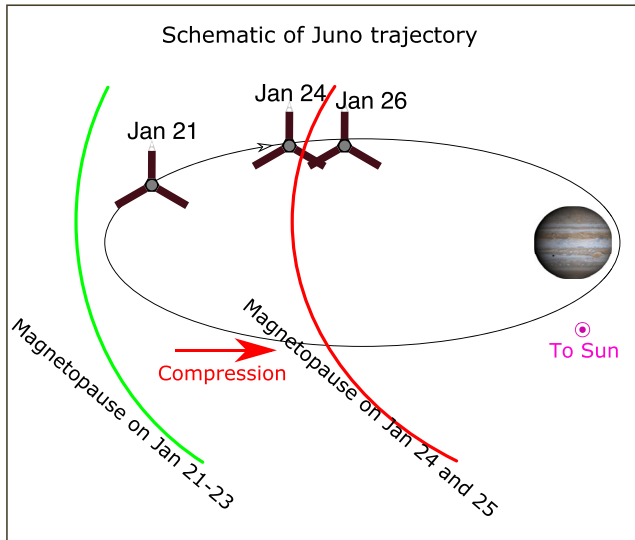


**Figure 4.** A sketch to illustrate Juno's trajectory and the locations of magnetopause before and after compression. Juno was inside the magnetosphere on 21–23 January and traveled into the magnetosheath on 24 January when the magnetopause was compressed. On 26 January, Juno was in the magnetopause boundary layer.

vertical dashed purple line) Juno's entry into the magnetosheath. The density increase is a naturally expected consequence of magnetopause compression (Gershman et al., 2017; Hospodarsky et al., 2017; Kurth et al., 2002), confirming our determination of compression from the appearance (or disappearance) of the trapped continuum radiation. The magnetic field components and magnetic strength from Juno (Figures 3c–3f) were nearly unperturbed before being approached by the magnetopause (as indicated by the first vertical dashed purple line), suggesting that during this period solar wind was relatively quiet. The ADS event on 22 January (Figure 2a) and subsequent quiet auroral morphology (Figure 2b) occur during the same solar wind conditions, that is, relatively quiet solar wind, showing that the ADS was not driven by solar wind compression. The two MAB images (Figures 2c and 2d) were both acquired during the compressed period (i.e., between the two vertical purple lines in Figure 3).

### 3.2. A Global Picture Drawn From a Large Data Set Between June 2016 and July 2017

We surveyed the HST data set from June 2016 to July 2017 when Juno was exploring the magnetosphere at  $>70 R_J$ , to seek a systematic relation between the compressed magnetopause and the two types of auroral morphologies (i.e., MAB and ADS), using the same criteria detailed in Sections 2.2 and 3.1, for the auroral morphology and magnetospheric conditions respectively. As shown in Table 1, we have identified eight auroral events with coordinated Juno's in situ measurements and HST's remote sensing of aurorae (with an

exception event on 19 March 2017). Three of them are ADS morphology, and the other five are MAB morphology (see Figure S2 in Supporting Information S1 for other auroral events that are not shown in the main text). Note that the 19 March event lasted for four successive days while the uncertainty of solar wind propagation is less than 2 days, therefore this event provides an excellent opportunity to apply a model of the solar wind at Jupiter during a MAB event with a strong level of confidence. As shown in Figure S2 in Supporting Information S1, the polar emissions and injection auroras are not uniform either for MAB or ADS, suggesting that these emissions are highly dynamic and not well controlled by solar wind conditions. As we introduced in the 22–24 January 2017 case study, the mean arc width and the variation parameters can be used to characterize each type of auroral morphology. The empirical numbers of mean arc width and variation are described above. The quiet aurora morphology is empirically defined as total auroral power below 1,200 GW, and the maximum brightness to be lower than 1,000 kiloRayleighs on dawn side main auroral oval. It is noteworthy that these thresholds are empirical and based on a limited number of cases. A further statistical study using many more observations are important to refine the criteria. The enhanced solar wind compression was given by Tao model prediction (Tao et al., 2005) for the event on 19 March 2017, and the auroral morphology is a typical MAB, consistent with the other five events, whose magnetopause compression were directly determined by plasma waves.

As detailed in the Figures S3, S4, and S5 in Supporting Information S1, Juno detected the compressed magnetopause before the MAB events were observed and remained in the magnetosheath during the auroral event, which supports the simultaneity of magnetopause compression and MAB events. In one unique case, the compression event could not be established with the same level of certainty. Indeed, for the event on 30 June 2016, a gap in the wave data prevents us to fully confirm the compression level of the magnetopause. Nevertheless, we note that 4 hr prior to this auroral event, Juno was still in the magnetosheath at  $\sim 73 R_J$ , indicating that the magnetopause was strongly compressed at about 4 hr (i.e., less than half a Jovian rotation) before the auroral event. It is challenging to precisely determine the time for the magnetopause crossings, especially for the cases during which Juno remained close to the magnetopause boundary for a while. However, the present study does not depend on the accurate determinations of the magnetopause crossings. Instead, the partial magnetopause crossings or encountering magnetopause boundary layer are sufficient to indicate magnetopause compression (Gershman et al., 2017). We used the model of Joy et al. (2002) to simulate the location of the magnetopause under several levels of compression, as shown in Figure 5. The location of the Juno magnetopause crossings corresponds to dynamic pressures as high as 0.2–0.4 nPa for all MAB events. The expected dynamic pressures are much higher than the nominal pressure of 0.09 nPa, thus these events correspond to substantial solar wind compressions.

**Table 1**  
*The Event List for ADS and MAB Auroral Morphologies*

Events <b>a</b>	Compression? If yes, time and locations of the magnetopause encounter	Juno location ( $R_J$ )	Arc width/variation (km)
<b>ADS events</b>			
2016/07/18 18:58 UT	Yes, 2016/07/17 00:09 UT, at 91 $R_J$ Until 2016/07/19 17:50 UT	96	2194/958
2017/01/22 15:31 UT	No	86	1,468/548
2017/04/23 14:00 UT	No	113	1,714/641
<b>MAB events <b>b</b></b>			
2016/06/30 04:13 UT	Yes, 2016/06/29 17:15 UT, at 76 $R_J$ Until 2016/06/29 23:40 UT	72	825/341
2016/07/14 16:23 UT <sup>c</sup>	Yes, 2016/07/14 12:39 UT, at 80 $R_J$ Until 2016/07/14 15:20 UT	81	790/278
2016/07/17 14:21 UT	Yes, 2016/07/17 00:09 UT, at 91 $R_J$ Until 2016/07/19 17:50 UT	92	830/289
2017/01/24 15:11 UT <sup>d</sup>	Yes, 2017/01/24 08:30 UT, at 79 $R_J$ Until 2017/01/25 17:50 UT	78	626/262
2017/03/19 09:57 UT <sup>e</sup>	Yes, inferred from modeling	74	639/385

<sup>a</sup>The events were selected from 2016 June to 2017 July, when Juno was at  $>70 R_J$  and simultaneous auroral images were available from HST. In case of successive auroral sequences with the same morphology, we grouped these sequences in Table 1 for clarity reasons, but all individual sequences are reported in Table S1 in Supporting Information S1. <sup>b</sup>Note that the two MAB events on 14 and 17 July 2016 may be grouped as a long-lasting solar wind compression event, but we could not confirm if the magnetopause or auroral morphology in between have returned to quiet condition. <sup>c</sup>At  $\sim 14$  July 2016 12:39 UT, Juno encountered the magnetopause boundary layer, and clearly entered into the magnetosheath at 21:19 UT (Ranquist et al., 2019). <sup>d</sup>At  $\sim 24$  January 2017 08:30 UT, Juno encountered the magnetopause boundary layer, and clearly entered into the magnetosheath at 25 January 2017 00 UT. <sup>e</sup>This auroral event and the solar wind compression condition are analyzed in details by Yao et al. (2019).

We further surveyed all HST visits when Juno was located between 70 and 120  $R_J$  between June 2016 and June 2017. Table S1 and Figure S6 in Supporting Information S1 show all dim, ADS and MAB events. The dim events are auroral morphologies showing low activities following the classification (i.e., family index 1 and 2 in Grodent et al. (2018)). From the whole data set, we eventually identify 32 HST visits showing either dim, ADS or MAB morphologies. For 21 of these HST visits, we could confirm a compressed magnetopause (10 events) or an uncompressed magnetopause (11 events) and the 11 remaining events are too ambiguous to call. Key results are summarized as: (a) for the 11 events during the uncompressed magnetopause condition, we found 9 of them to be dim morphology and 2 to be ADS without a clear afternoon/dusk-side brightening; (b) for the 10 events during the confirmed magnetopause compression condition, 8 of them are MAB, and two of them are ADS. However, for the two ADS events during compression, the brightness of the noon and afternoon/dusk sides of the main aurora was also enhanced, indicative of a superposition of an ADS on top of a MAB. Therefore, ADS could exist during quiet condition (ADS-Q) and compressional condition (ADS-MAB). There is no dim auroral morphology during solar wind compression, and all MAB events are observed during solar wind compression.

#### 4. Discussion

In this study, we focus on three types of auroral morphologies, that is, quiet, ADS and MAB. ADS and MAB are defined only based on dawn emissions. The afternoon/dusk emission in MAB events show enhancements which are distributed in a large range of latitudes, but we do not analyze the detailed features in this study. Using the solar wind conditions inferred by radio wave emissions, we investigate the effect of solar wind compression in driving auroral emissions. The unprecedented data set could also be used to understanding many other effects due to solar wind compression at Jupiter, for example, the low-frequency extension of kilometric wave that informs the altitude of auroral region.

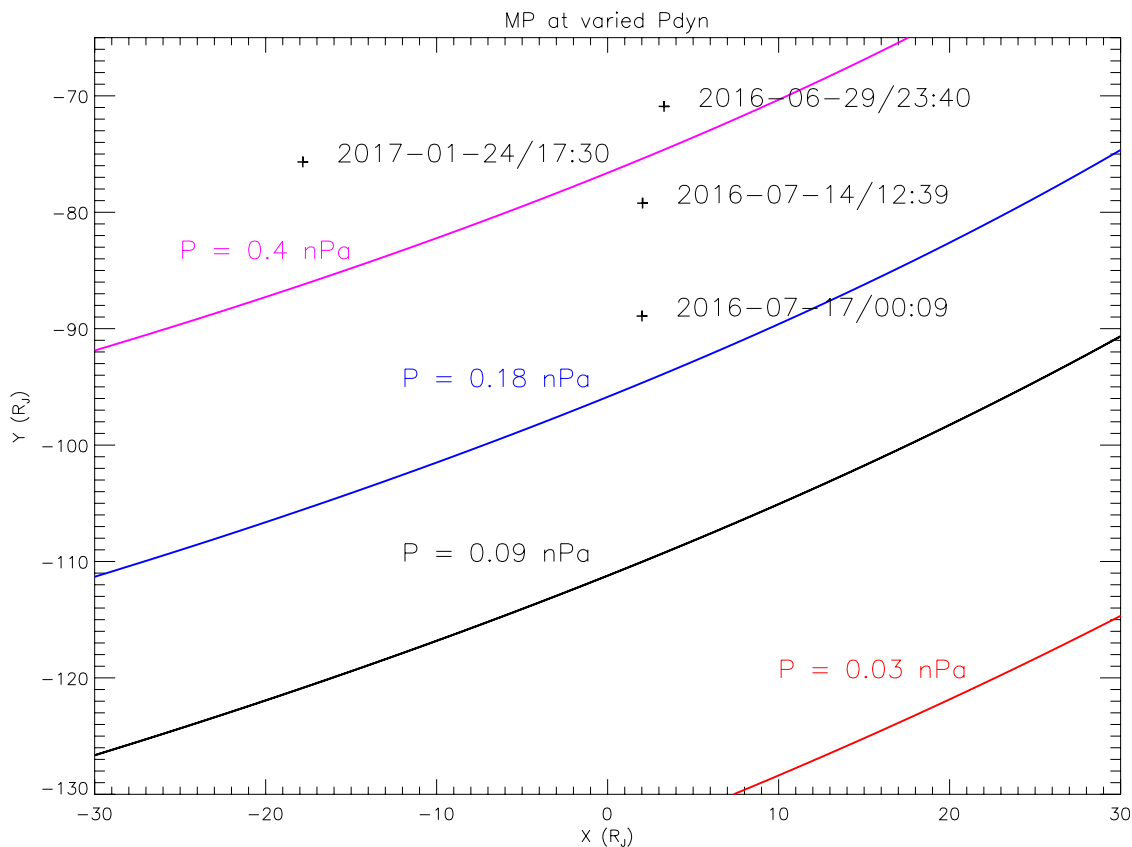


**Figure 5.** The magnetopause location in Jupiter-centered coordinate system under several typical dynamic pressure (0.03, 0.09, 0.18, and 0.4 nPa) based on the modeling relation in Joy et al. (2002). The nominal dynamic pressure is 0.09 nPa, whose magnetopause is the black curve. The Juno locations when crossing the magnetopause are marked with the plus signs. Note that the modeling results of solar wind dynamic pressure from Joy et al. (2002) model only represent the minimum solutions, because Juno could only detect the magnetopause that reached at least to the spacecraft, while it is unclear how much inward the magnetopause may have eventually reached.

The direct connection between auroral morphology and magnetopause compression conditions could also provide key insights to examine the existing hypothesis (e.g., corotation breakdown enforcement currents and Alfvénic Poynting flux). Radioti et al. (2008) have shown that the main auroral oval exhibits substantially reduced brightness near noon local time (e.g., clearly shown in Figures 2c and 2d). Traditionally, the auroral discontinuity is explained as a consequence of the shape of the dayside magnetosphere, which brings the magnetospheric plasma closer to the planet and accelerates its rotation, which reduces the corotation enforcement current and the related auroral precipitation in the pre-noon local time sector. For example, in a local-time dependent modeling study, Ray et al. (2014), who modeled the local time dependence of the auroral currents (but not its temporal evolution under magnetospheric compression), find that the auroral currents are modest in the post-noon sector, near 1400 LT. Consequently, the presence of this discontinuity in the main auroral emissions was considered as a piece of evidence supporting the corotation breakdown explanation for the main auroral oval (Cowley et al., 2005). However, we shall note that the main auroral emission in the model of Ray et al. (2014) is expected to be brighter in the dawnside than in the duskside, while the HST observations show that the duskside is averagely three times brighter than the dawnside (Bonfond et al., 2015). This results in this study indicate that the local time auroral distribution is very sensitive to solar wind compression, which provide important constraints in future modeling research.

It is particularly noteworthy that the auroral evolution shown in Figure 2 is contradictory with the modeling prediction that a solar wind compression would cause the aurora in the noon sector to dim even more than during quiet times. The quantitative analysis is shown in Figure 6. The evidence against the present models based on corotation enforcement theory is reviewed in a recent commentary paper (Bonfond et al., 2020). Vogt et al. (2019) analyzed the magnetic field bendback as a function of the propagated solar wind conditions at Jupiter

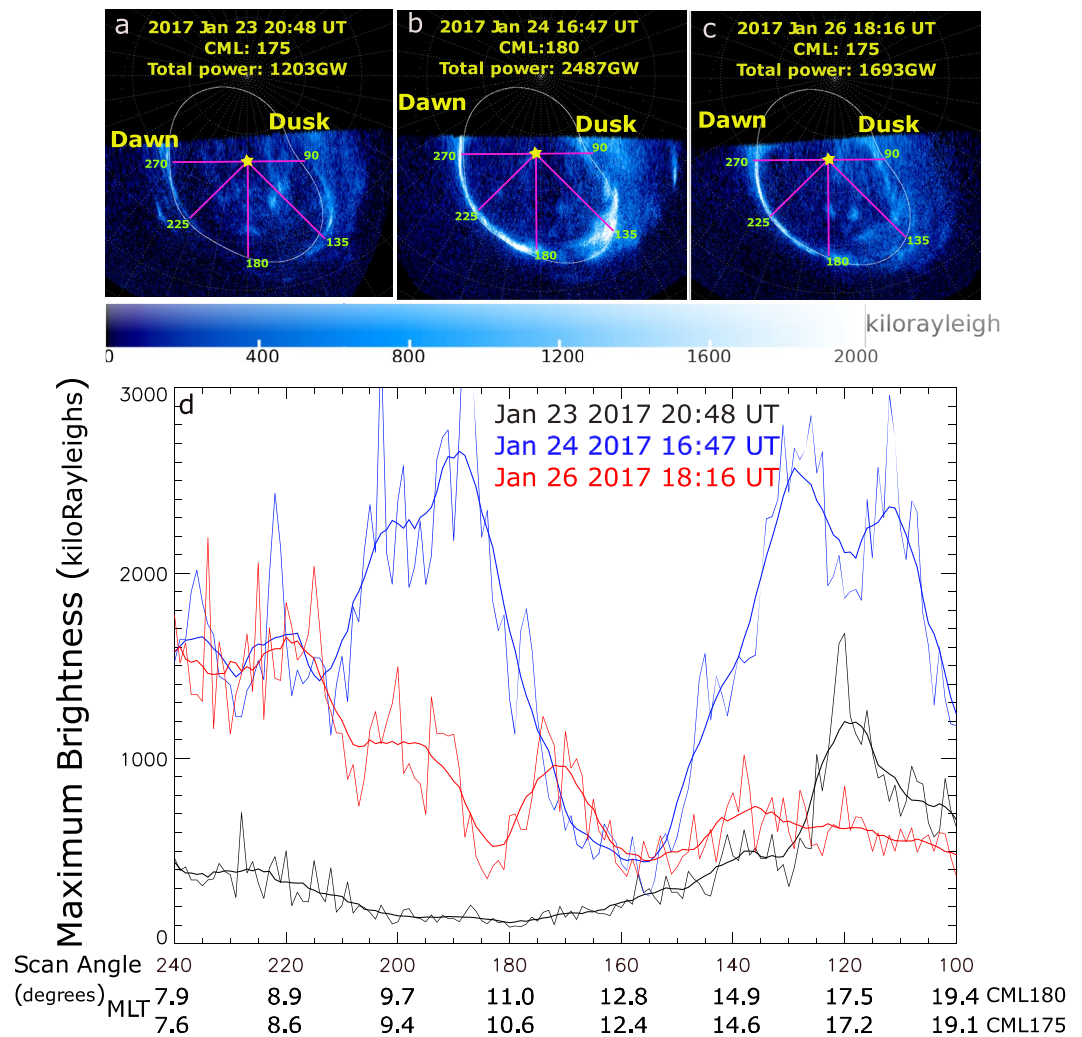


**Figure 6.** Comparisons between auroral brightness distributions before, during and after magnetopause compression. Top: three selected auroral images with similar viewing geometries. The yellow star indicates the morphological center of the main oval (System III longitude at  $185^\circ$  and latitude at  $74^\circ$ ) (Grodent et al., 2004), and the blue lines indicate scan angles at five given values. Bottom: distribution of maximum brightness as a function of scan angle for the three auroral images on the top panel during uncompressed magnetopause, compressed magnetopause and 2 days after the compression.

and they found that the bendback was increased at dawn and decreased at dusk during compressed conditions. They concluded that, according to the corotation enforcement current theory, the main auroral emissions should be increased at dawn and decreased at dusk under such conditions.

Figures 6a–6c show three selected images from the three HST visits (Figures 2b, 2d and 2e), but each image is integrated over 1 min. All the three images are acquired in a similar viewing geometry, that is, their average Central Meridian Longitudes (CML) are close (175, 180, and 175 respectively), which facilitates the comparison of the brightness profiles as a function of both local time and scan angle on the same plot. The magnetic local times obtained using flux equivalence model (Vogt et al., 2015, 2011) with JRM09 (Connerney et al., 2018) as an internal model, are overlaid along the scan angle. The slight difference in CML results in a difference of about 0.3 hr in MLT. As illustrated by the blue lines (original and smoothed over 10 points) during the compression event, the brightness in near noon local times ( $\sim 500$  kiloRayleighs at noon local times  $\sim 12.5$  LT) is much lower than dawn local times (higher than 2,600 kiloRayleighs at dawn local times  $\sim 10$ – $10.5$  LT) and afternoon/dusk local times (higher than 2,600 kiloRayleighs at afternoon/dusk local times  $\sim 16$  LT). The change is as large as 70 kiloRayleighs per degree. In contrast to the compressional period, the variation of auroral brightness along the main oval during quiet period (the black curve) is only  $\sim 10$  kiloRayleighs per degree. Although solar wind

compression enhanced the near noon auroral discontinuity (i.e., the gradient of auroral intensity) by a factor of 7, the observations do not support the hypothesis that solar wind compression dim near noon aurora. Oppositely, the auroral brightness in auroral discontinuity region also increased, although not by as much as both sides of the discontinuity, which is why the discontinuity becomes clearly visible. The MAB auroral discontinuity is near magnetic noon, and the quiet time auroral discontinuity is centered at about 10 MLT (See the black lines in Figure 6 and Table 2 in Supporting Information S1 for all other events). The magnetic local time may be related to plasma circulation or some special magnetic configuration to be discovered. In contrast with the substantial near-noon enhancement of the auroral emission shown in Figure 6, numerical magnetohydrodynamic simulations predict either a small enhancement of field-aligned currents (Chané et al., 2017) or reduced field-aligned currents (Sarkango et al., 2019) in the near-noon sector during solar wind compressions. The discrepancies among the different simulation results and the observations shall be further investigated in future modeling studies of the Jupiter's magnetosphere. The time-varying modeling results (Cowley et al., 2007) predict that the magnetosphere would re-establish a steady state after 1–2 days of compression and the main aurora would be fainter than pre-compression state. This is, however, not supported by the auroral image shown in Figure 6. This inconsistency was also revealed by Nichols et al. (2017a).

We shall point out that enhanced auroral events during solar wind compression do not directly conflict with the auroral current reduction in the noon and afternoon/dusk sectors associated with corotation breakdown enforcement mechanism. It is possible that several mechanisms contribute to the main emissions and that the reduction of the corotation enforcement currents during compression is masked by the large increase in broadband precipitation, that is, Alfvénic acceleration, arising for other processes, such as turbulence (Saur, 2004) and the Landau damping of kinetic Alfvén wave (Saur et al., 2018). A recent study using simultaneous observations of Alfvén waves from Juno and auroras from HST reveals a positive correlation between the Ultralow-frequency waves and auroral emissions (Pan et al., 2021), strongly suggesting that Alfvén waves is a major source of Jupiter's main aurora. The compression of magnetosphere is recently confirmed to produce intense Poynting flux and power aurora at Earth (Keiling et al., 2019), which may provide an important implication to understand the connection between MAB and solar wind compression (Delamere & Bagenal, 2010). Because of the size and rotationally dominated dynamics of the Jovian magnetosphere and unlike the terrestrial auroral response to solar wind compression, it may take some time to form Jupiter's MAB (i.e., several hours), and the MAB events may last for substantial duration (a few days). Therefore, MAB auroral morphology during solar wind compression might not be directly driven by the corotation breakdown enforcement current, but resulting instead from the impact of the reduced volume of the magnetosphere and the stronger shear on its flanks on the internal dynamics at Jupiter. This may explain the delay of the auroral response observed by Kita et al. (2019). A global statistical comparison between auroral emissions and Alfvén waves, together with global numerical simulation would greatly benefit the understanding of Alfvénic acceleration in generating the main aurora.

Using the accurate determination of magnetopause compression and the contemporaneous auroral observation from HST, we show a systematic connection between the MAB auroral morphology and solar wind compression, while ADS could occur during both quiet and enhanced solar wind periods (Bonfond et al., 2021; Kimura et al., 2015, 2017; Nichols, Yeoman, et al., 2017; Nichols et al., 2009). ADS events are substantially extended to lower latitudes, which may imply that energy sources for ADS span a large radial range from the middle to inner magnetosphere. We notice that the hectometric radio emission was enhanced during all MAB events as reported in previous literature (Echer et al., 2010; Gurnett et al., 2002), but not during the two ADS events on 22 January 2017 and 23 April 2017, when the magnetopause was not compressed (Table S2 in Supporting Information S1). The relationship between radio emission and UV auroral morphologies could provide insights in understanding the auroral driving mechanisms, although we also notice that the radio enhancement (i.e., hectometric emissions) may last for longer time than UV aurora, which has also been reported in the literature (Gurnett et al., 2002; Hess et al., 2014). Further studies on their detailed relations are probably important to understand their systematic connections to solar wind compressions. The differences in how solar wind compressions drive aurorae at Jupiter reflect fundamental processes of energy circulation in Jupiter's magnetosphere.

During a compression event, the aurora systematically brightens at dawn (and at noon and afternoon/dusk as well while distributed in a large range of latitude). In the corotation breakdown enforcement current hypothesis, intense auroral current will require large azimuthal bendback of magnetic fields, which however, does not show a highly consistent trend (i.e., events with more swept back were roughly twice as common as events toward sweep forward) (Vogt et al., 2019). We shall also notice that an alternative auroral source, that is, the Alfvénic

Poynting flux (Chaston et al., 1999, 2007; Keiling et al., 2003, 2019), could be strongly enhanced during solar wind compression and produce strong auroral emission, is not directly related to the degree of bendback.

There are also secondary auroral variations during solar wind compression. Yao et al. (2019) revealed the correlation between magnetic unloading process (i.e., time-varying) and main auroral enhancement, and the auroral emissions during either the loading phase and unloading phase are generally more bright than during quiet times, that is, the primary auroral response to solar wind compression. These results prove that the auroral emissions could not be fully described by a steady-state model. The same magnetic configuration with different evolving trends shall correspond to different auroral emissions. For example, a similar magnetic configuration may occur during magnetic loading and unloading processes, while the auroral emission during unloading is higher than during the loading process. This comparison is analogous to the magnetospheric responses to solar wind compression. For a short time, the magnetopause may have the same intermediate shape and standoff distance during a compression and relaxation, while the energization processes (e.g., auroral precipitation) are expected to be very different. This is because these energy dissipations are time-varying processes, so that they could not be well described by a steady-state model.

Finally, we would like to highlight some similarities between the auroral emissions at Saturn and Jupiter. During solar wind compression, Saturn's auroral emission is also expected to enhance (Clarke et al., 2009; Stallard et al., 2012). Therefore, the aurorae at terrestrial and jovian-like planets are all expected to increase during solar wind compression, regardless of their different mass sources and rotation speeds. The terrestrial explosive auroral intensification (known as auroral substorm) usually occurs near midnight, as a consequence of magnetotail collapse. Jupiter and Saturn often show strong auroral intensification on the dawn side, which is probably related to the rotationally driven magnetic reconnection and plasma circulation associated with Vasyliunas circle (Vasyliunas, 1983). Moreover, a recent comparison between Saturn's mean and median northern ultraviolet auroral brightness show that the median brightness on the dusk side is higher than the dawnside, suggesting a systematic mechanism in producing more aurora on the dusk. The mean value of Saturn's dawn aurora is much higher than the dusk, which is due to many transient auroral intensification, like ADS at Jupiter (Bader et al., 2019). Comparative analysis of auroral processes is valuable to understand planetary auroral in a global picture.

## 5. Conclusions

In this study, we analyze simultaneous observations from Juno and HST, to directly assess variations of the auroral morphology as a function of the compression state of the magnetosphere. Our main results are summarized:

1. We classify auroral brightening events as ADS and MAB, mainly based on the morphologies on the dawn sector. These events are not mutually exclusive.
2. MAB events are a consequence of magnetopause compression, and no MAB has been found during expanded magnetopause conditions.
3. ADS events are identified during either expanded or compressed magnetopause conditions. Magnetic reconnection and plasma instability in the night magnetotail are probably responsible for ADS events.
4. During expanded magnetopause conditions, the auroral morphologies are either dim or ADS. As shown in Table S1 and Figure S6 in Supporting Information S1, dim auroral morphology was only identified during quiet or unknown solar wind conditions. There was no dim auroral morphology event during magnetopause compression.
5. The near noon auroral discontinuity in MAB events is formed because of main auroral enhancements in the morning and afternoon sectors during magnetopause compression. The near noon aurora was not dimmed but slightly enhanced, which provide key constraints to modeling and simulation research. The center of auroral discontinuity moves from ~10 LT during quiet time to ~12 LT during MAB, which may provide useful constraint to understand the driver of auroral brightening during compression.

## Data Availability Statement

The auroral images are based on observations with the NASA/ESA HST (program HST GO-14105 and GO-14634), obtained at the Space Telescope Science Institute (STScI), which is operated by AURA for NASA. All data are publicly available at STScI via <https://archive.stsci.edu/hst/>. All Juno data presented here are publicly available from NASA's Planetary Data System (<https://pds-ppi.igpp.ucla.edu/>). The MAG data set

is available via <https://pds-ppi.igpp.ucla.edu/search/view/?f=yes%26id=pds://PPI/JNO-J-3-FGM-CAL-V1.0>, and the Wave data set is available via [https://pds-ppi.igpp.ucla.edu/search/view/?f=yes%26id=pds://PPI/JNO-E\\_J\\_SS-WAV-2-EDR-V1.0](https://pds-ppi.igpp.ucla.edu/search/view/?f=yes%26id=pds://PPI/JNO-E_J_SS-WAV-2-EDR-V1.0).

### Acknowledgments

Z.Y. acknowledges National Key R&D Program of China No. 2021YFA0718600, the National Science Foundation of China (Grant 42074211) and Key Research Program of the Institute of Geology & Geophysics CAS (grant IGGCAS-201904). B.B. is a Research Associate of the Fonds de la Recherche Scientifique—FNRS. We are grateful to NASA and contributing institutions which have made the Juno mission possible. This work was funded by NASA's New Frontiers Program for Juno via contract with the Southwest Research Institute. B.B., D.G., B.P. and R.L.G. acknowledge financial support from the Belgian Federal Science Policy Office (BELSPO) via the PRODEX Programme of ESA. The research at the University of Iowa was supported by NASA through Contract 699041X with Southwest Research Institute. The authors wish to thank the International Space Science Institute in Beijing (ISSI-BJ) for supporting and hosting the meetings of the International Team on "The morphology of auroras at Earth and giant planets: characteristics and their magnetospheric implications", during which the discussions leading/ contributing to this publication were held.

### References

- Bader, A., Badman, S., Cowley, S., Yao, Z., Ray, L. C., Kinrade, J., et al. (2019). The dynamics of Saturn's main aurorae. *Geophysical Research Letters*, *46*(17–18), 10283–10294. <https://doi.org/10.1029/2019GL084620>
- Ballester, G. E., Clarke, J. T., Trauger, J. T., Harris, W. M., Stapelfeldt, K. R., Crisp, D., et al. (1996). Time-resolved observations of Jupiter's far-ultraviolet aurora. *Science*, *274*(5286), 409–413. <https://doi.org/10.1126/science.274.5286.409>
- Baron, R., Owen, T., Connerney, J., Satoh, T., & Harrington, J. (1996). Solar wind control of Jupiter's H+3 auroras. *Icarus*, *120*(2), 437–442. <https://doi.org/10.1006/icar.1996.0063>
- Bonfond, B., Grodent, D., Gérard, J. C., Stallard, T., Clarke, J. T., Yoneda, M., et al. (2012). Auroral evidence of Io's control over the magnetosphere of Jupiter. *Geophysical Research Letters*, *39*(1), L01105. <https://doi.org/10.1029/2011GL050253>
- Bonfond, B., Gustin, J., Gérard, J.-C., Grodent, D., Radioti, A., Palmaerts, B., et al. (2015). The far-ultraviolet main auroral emission at Jupiter-Part 1: Dawn-dusk brightness asymmetries. *Annales Geophysicae*, *33*(10), 1203–1209. <https://doi.org/10.5194/angeo-33-1203-2015>
- Bonfond, B., Yao, Z., & Grodent, D. (2020). Six pieces of evidence against the corotation enforcement theory to explain the main aurora at Jupiter. *Journal of Geophysical Research: Space Physics*, *125*(11), e2020JA028152. <https://doi.org/10.1029/2020ja028152>
- Bonfond, B., Yao, Z. H., Gladstone, G. R., Grodent, D., Gerard, J., Matar, J., et al. (2021). Are dawn storms Jupiter's auroral substorms? *AGU Advances*, *2*(1), e2020AV000275. <https://doi.org/10.1029/2020AV000275>
- Chané, E., Saur, J., Keppens, R., & Poedts, S. (2017). How is the Jovian main auroral emission affected by the solar wind? *Journal of Geophysical Research: Space Physics*, *122*(2), 1960–1978. <https://doi.org/10.1002/2016JA023318>
- Chaston, C., Carlson, C., McFadden, J., Ergun, R., & Strangeway, R. (2007). How important are dispersive Alfvén waves for auroral particle acceleration? *Geophysical Research Letters*, *34*(7), L07101. <https://doi.org/10.1029/2006GL029144>
- Chaston, C., Carlson, C., Peria, W., Ergun, R., & McFadden, J. (1999). FAST observations of inertial Alfvén waves in the dayside aurora. *Geophysical Research Letters*, *26*(6), 647–650. <https://doi.org/10.1029/1998GL900246>
- Clarke, J., Nichols, J., Gérard, J. C., Grodent, D., Hansen, K., Kurth, W., et al. (2009). Response of Jupiter's and Saturn's auroral activity to the solar wind. *Journal of Geophysical Research*, *114*(A5), A05210. <https://doi.org/10.1029/2008JA013694>
- Clarke, J. T., Ballester, G., Trauger, J., Ajello, J., Pryor, W., Tobiska, K., et al. (1998). Hubble Space Telescope imaging of Jupiter's UV aurora during the Galileo orbiter mission. *Journal of Geophysical Research*, *103*(E9), 20217–20236. <https://doi.org/10.1029/98je01130>
- Connerney, J., Bann, M., Bjarno, J., Denver, T., Espley, J., Jørgensen, J., et al. (2017). The Juno magnetic field investigation. *Space Science Reviews*, *213*(1–4), 39–138. <https://doi.org/10.1007/s11214-017-0334-z>
- Connerney, J., Kotsiaros, S., Oliverson, R., Espley, J., Jørgensen, J. L., Joergensen, P., et al. (2018). A new model of Jupiter's magnetic field from Juno's first nine orbits. *Geophysical Research Letters*, *45*(6), 2590–2596. <https://doi.org/10.1002/2018GL077312>
- Connerney, J., & Satoh, T. (2000). The H3+ ion: A remote diagnostic of the Jovian magnetosphere. *Philosophical Transactions of the Royal Society of London, Series A: Mathematical, Physical and Engineering Sciences*, *358*(1774), 2471–2483. <https://doi.org/10.1098/rsta.2000.0661>
- Cowley, S., Alexeev, I., Belenkaya, E., Bunce, E., Cottis, C., Kalegaev, V., et al. (2005). A simple axisymmetric model of magnetosphere-ionosphere coupling currents in Jupiter's polar ionosphere. *Journal of Geophysical Research*, *110*(A11), A11209. <https://doi.org/10.1029/2005JA011237>
- Cowley, S., & Bunce, E. (2001). Origin of the main auroral oval in Jupiter's coupled magnetosphere-ionosphere system. *Planetary and Space Science*, *49*(10–11), 1067–1088. [https://doi.org/10.1016/S0032-0633\(00\)00167-7](https://doi.org/10.1016/S0032-0633(00)00167-7)
- Cowley, S., Nichols, J., & Andrews, D. J. (2007). Modulation of Jupiter's plasma flow, polar currents, and auroral precipitation by solar wind-induced compressions and expansions of the magnetosphere: A simple theoretical model. *Annals of Geophysics*, *25*(6), 1433–1463. <https://doi.org/10.5194/angeo-25-1433-2007>
- Damiano, P. A., Delamere, P. A., Stauffer, B., Ng, C.-S., & Johnson, J. R. (2019). Kinetic simulations of electron acceleration by dispersive scale Alfvén waves in Jupiter's magnetosphere. *Geophysical Research Letters*, *46*(6), 3043–3051. <https://doi.org/10.1029/2018GL081219>
- Delamere, P., & Bagenal, F. (2010). Solar wind interaction with Jupiter's magnetosphere. *Journal of Geophysical Research*, *115*(A10), A10201. <https://doi.org/10.1029/2010JA015347>
- Dunn, W., Branduardi-Raymont, G., Ray, L., Jackman, C., Kraft, R., Elsner, R., et al. (2017). The independent pulsations of Jupiter's northern and southern X-ray auroras. *Nature Astronomy*, *1*(11), 758–764. <https://doi.org/10.1038/s41550-017-0262-6>
- Dunn, W. R., Branduardi-Raymont, G., Elsner, R. F., Vogt, M. F., Lamy, L., Ford, P. G., et al. (2016). The impact of an ICME on the Jovian X-ray aurora. *Journal of Geophysical Research: Space Physics*, *121*(3), 2274–2307. <https://doi.org/10.1002/2015JA021888>
- Echer, E., Zarka, P., Gonzalez, W., Morioka, A., & Denis, L. (2010). Solar wind effects on Jupiter non-Io DAM emissions during Ulysses distant encounter (2003–2004). *Astronomy & Astrophysics*, *519*, A84. <https://doi.org/10.1051/0004-6361/200913305>
- Fränz, M., & Harper, D. (2002). Heliospheric coordinate systems. *Planetary and Space Science*, *50*(2), 217–233. [https://doi.org/10.1016/S0032-0633\(01\)00119-2](https://doi.org/10.1016/S0032-0633(01)00119-2)
- Gershman, D. J., Connerney, J. E., Kotsiaros, S., DiBraccio, G. A., Martos, Y. M., Viñas, A. F., et al. (2019). Alfvénic fluctuations associated with Jupiter's auroral emissions. *Geophysical Research Letters*, *46*(13), 7157–7165. <https://doi.org/10.1029/2019GL082951>
- Gershman, D. J., DiBraccio, G. A., Connerney, J. E., Hospodarsky, G., Kurth, W. S., Ebert, R. W., et al. (2017). Juno observations of large-scale compressions of Jupiter's dawnside magnetopause. *Geophysical Research Letters*, *44*(15), 7559–7568. <https://doi.org/10.1002/2017GL073132>
- Gladstone, G., Waite, J., Grodent, D., Lewis, W., Cray, F., Elsner, R. F., et al. (2002). A pulsating auroral X-ray hot spot on Jupiter. *Nature*, *415*(6875), 1000–1003. <https://doi.org/10.1038/4151000a>
- Grodent, D. (2015). A brief review of ultraviolet auroral emissions on giant planets. *Space Science Reviews*, *187*(1–4), 23–50. <https://doi.org/10.1007/s11214-014-0052-8>
- Grodent, D., Bonfond, B., Yao, Z., Gérard, J. C., Radioti, A., Dumont, M., et al. (2018). Jupiter's aurora observed with HST during Juno orbits 3 to 7. *Journal of Geophysical Research: Space Physics*, *123*(5), 3299–3319. <https://doi.org/10.1002/2017JA025046>
- Grodent, D., Clarke, J., Waite, J., Cowley, S., Gérard, J. C., & Kim, J. (2003). Jupiter's polar auroral emissions. *Journal of Geophysical Research*, *108*(A10), 1366. <https://doi.org/10.1029/2003JA010017>
- Grodent, D., Gérard, J. C., Clarke, J., Gladstone, G., & Waite, J. (2004). A possible auroral signature of a magnetotail reconnection process on Jupiter. *Journal of Geophysical Research*, *109*(A5), A05201. <https://doi.org/10.1029/2003JA010341>
- Gurnett, D., Kurth, W., Hospodarsky, G., Persoon, A., Zarka, P., Lecacheux, A., et al. (2002). Control of Jupiter's radio emission and aurorae by the solar wind. *Nature*, *415*(6875), 985–987. <https://doi.org/10.1038/415985a>

- Gurnett, D., Kurth, W., & Scarf, F. (1980). The structure of the Jovian magnetotail from plasma wave observations. *Geophysical Research Letters*, 7(1), 53–56. <https://doi.org/10.1029/GL007i001p00053>
- Gustin, J., Bonfond, B., Grodent, D., & Gérard, J.-C. (2012). Conversion from HST ACS and STIS auroral counts into brightness, precipitated power, and radiated power for H2 giant planets. *Journal of Geophysical Research*, 117(A7), A07316. <https://doi.org/10.1029/2012JA017607>
- Haggerty, D., Mauk, B., Paranicas, C., Clark, G., Kollmann, P., Rymer, A., et al. (2019). Jovian injections observed at high latitude. *Geophysical Research Letters*, 46(16), 9397–9404. <https://doi.org/10.1029/2019GL083442>
- Hess, S., Echer, E., Zarka, P., Lamy, L., & Delamere, P. (2014). Multi-instrument study of the Jovian radio emissions triggered by solar wind shocks and inferred magnetospheric subcorotation rates. *Planetary and Space Science*, 99, 136–148. <https://doi.org/10.1016/j.pss.2014.05.015>
- Hill, T. (1979). Inertial limit on corotation. *Journal of Geophysical Research*, 84(A11), 6554–6558. <https://doi.org/10.1029/JA084iA11p06554>
- Hill, T. (2001). The Jovian auroral oval. *Journal of Geophysical Research*, 106(A5), 8101–8107. <https://doi.org/10.1029/2000JA000302>
- Hospodarsky, G., Kurth, W., Bolton, S., Allegrini, F., Clark, G., Connerney, J., et al. (2017). Jovian bow shock and magnetopause encounters by the Juno spacecraft. *Geophysical Research Letters*, 44(10), 4506–4512. <https://doi.org/10.1002/2017GL073177>
- Joy, S., Kivelson, M., Walker, R., Khurana, K., Russell, C., & Ogino, T. (2002). Probabilistic models of the Jovian magnetopause and bow shock locations. *Journal of Geophysical Research*, 107(A10), 1309. <https://doi.org/10.1029/2001JA009146>
- Keiling, A., Thaller, S., Wygant, J., & Dombeck, J. (2019). Assessing the global Alfvén wave power flow into and out of the auroral acceleration region during geomagnetic storms. *Science Advances*, 5(6), eaav8411. <https://doi.org/10.1126/sciadv.aav8411>
- Keiling, A., Wygant, J., Cattell, C., Mozer, F., & Russell, C. (2003). The global morphology of wave Poynting flux: Powering the aurora. *Science*, 299(5605), 383–386. <https://doi.org/10.1126/science.1080073>
- Kimura, T., Badman, S., Tao, C., Yoshioka, K., Murakami, G., Yamazaki, A., et al. (2015). Transient internally driven aurora at Jupiter discovered by Hisaki and the Hubble space telescope. *Geophysical Research Letters*, 42(6), 1662–1668. <https://doi.org/10.1002/2015GL063272>
- Kimura, T., Nichols, J. D., Gray, R., Tao, C., Murakami, G., Yamazaki, A., et al. (2017). Transient brightening of Jupiter's aurora observed by the Hisaki satellite and Hubble Space Telescope during approach phase of the Juno spacecraft. *Geophysical Research Letters*, 44(10), 4523–4531. <https://doi.org/10.1002/2017GL072912>
- Kita, H., Kimura, T., Tao, C., Tsuchiya, F., Misawa, H., Sakanoi, T., et al. (2016). Characteristics of solar wind control on Jovian UV auroral activity deciphered by long-term Hisaki EXCEED observations: Evidence of preconditioning of the magnetosphere? *Geophysical Research Letters*, 43(13), 6790–6798. <https://doi.org/10.1002/2016GL069481>
- Kita, H., Kimura, T., Tao, C., Tsuchiya, F., Murakami, G., Yamazaki, A., et al. (2019). Jovian UV aurora's response to the solar wind: Hisaki EXCEED and Juno observations. *Journal of Geophysical Research: Space Physics*(124), 10209–10218. <https://doi.org/10.1029/2019JA026997>
- Korth, H., Zhang, Y., Anderson, B. J., Sotiirelis, T., & Waters, C. L. (2014). Statistical relationship between large-scale upward field-aligned currents and electron precipitation. *Journal of Geophysical Research: Space Physics*, 119(8), 6715–6731. <https://doi.org/10.1002/2014JA019961>
- Kurth, W., Barbosa, D., Scarf, F., Gurnett, D., & Poynter, R. (1979). Low frequency radio emissions from Jupiter: Jovian kilometric radiation. *Geophysical Research Letters*, 6(9), 747–750. <https://doi.org/10.1029/GL006i009p00747>
- Kurth, W., Gurnett, D., Hospodarsky, G., Farrell, W., Roux, A., Dougherty, M., et al. (2002). The dusk flank of Jupiter's magnetosphere. *Nature*, 415(6875), 991–994. <https://doi.org/10.1038/415991a>
- Kurth, W., Hospodarsky, G., Kirchner, D., Mokrzycki, B., Averkamp, T., Robison, W., et al. (2017). The Juno waves investigation. *Space Science Reviews*, 213(1–4), 347–392. <https://doi.org/10.1007/s11214-017-0396-y>
- Lysak, R. L., & Song, Y. (2020). Field line resonances in Jupiter's magnetosphere. *Geophysical Research Letters*, 47(18), e2020GL089473. <https://doi.org/10.1029/2020GL089473>
- Mauk, B., & Bagenal, F. (2013). Comparative auroral physics: Earth and other planets, *auroral Phenomenology and magnetospheric processes: Earth and other planets* (pp. 3–26). <https://doi.org/10.1029/2011GM001192>
- Mauk, B., Clarke, J., Grodent, D., Waite, J., Jr., Paranicas, C., & Williams, D. (2002). Transient aurora on Jupiter from injections of magnetospheric electrons. *Nature*, 415(6875), 1003–1005. <https://doi.org/10.1038/4151003a>
- Mauk, B., Haggerty, D., Paranicas, C., Clark, G., Kollmann, P., Rymer, A., et al. (2017). Discrete and broadband electron acceleration in Jupiter's powerful aurora. *Nature*, 549(7670), 66–69. <https://doi.org/10.1038/nature23648>
- Newell, P., Sotiirelis, T., & Wing, S. (2009). Diffuse, monoenergetic, and broadband aurora: The global precipitation budget. *Journal of Geophysical Research*, 114(A9), A09207. <https://doi.org/10.1029/2009JA014326>
- Newell, P. T., Sotiirelis, T., & Wing, S. (2010). Seasonal variations in diffuse, monoenergetic, and broadband aurora. *Journal of Geophysical Research*, 115(A3), A03216. <https://doi.org/10.1029/2009JA014805>
- Nichols, J., Badman, S. V., Bagenal, F., Bolton, S., Bonfond, B., Bunce, E., et al. (2017). Response of Jupiter's auroras to conditions in the interplanetary medium as measured by the Hubble Space Telescope and Juno. *Geophysical Research Letters*, 44(15), 7643–7652. <https://doi.org/10.1002/2017GL073029>
- Nichols, J., Bunce, E., Clarke, J. T., Cowley, S., Gérard, J. C., Grodent, D., & Pryor, W. R. (2007). Response of Jupiter's UV auroras to interplanetary conditions as observed by the Hubble Space Telescope during the Cassini flyby campaign. *Journal of Geophysical Research*, 112(A2), A02203. <https://doi.org/10.1029/2006JA012005>
- Nichols, J., Yeoman, T., Bunce, E., Chowdhury, M., Cowley, S., & Robinson, T. (2017). Periodic emission within Jupiter's main auroral oval. *Geophysical Research Letters*, 44(18), 9192–9198. <https://doi.org/10.1002/2017GL074824>
- Nichols, J. D., Clarke, J. T., Gérard, J. C., Grodent, D., & Hansen, K. C. (2009). Variation of different components of Jupiter's auroral emission. *Journal of Geophysical Research*, 114(A6), A06210. <https://doi.org/10.1029/2009JA014051>
- Nichols, J. D., Kamran, A., & Milan, S. E. (2019). Machine learning analysis of Jupiter's far-ultraviolet auroral morphology. *Journal of Geophysical Research: Space Physics*, 124(11), 8884–8892. <https://doi.org/10.1029/2019JA027120>
- Pan, D.-X., Yao, Z.-H., Manners, H., Dunn, W., Bonfond, B., Grodent, D., et al. (2021). Ultralow-frequency waves in driving Jovian aurorae revealed by observations from HST and Juno. *Geophysical Research Letters*, 48(5), e2020GL091579. <https://doi.org/10.1029/2020GL091579>
- Prangé, R., Chagnon, G., Kivelson, M. G., Livengood, T. A., & Kurth, W. (2001). Temporal monitoring of Jupiter's auroral activity with IUE during the Galileo mission. Implications for magnetospheric processes. *Planetary and Space Science*, 49(3–4), 405–415. [https://doi.org/10.1016/S0032-0633\(00\)00161-6](https://doi.org/10.1016/S0032-0633(00)00161-6)
- Prangé, R., Pallier, L., Hansen, K. C., Howard, R., Vourlidis, A., Courtin, R., & Parkinson, C. (2004). An interplanetary shock traced by planetary auroral storms from the Sun to Saturn. *Nature*, 432(7013), 78–81. <https://doi.org/10.1038/nature02986>
- Radioti, A., Gérard, J. C., Grodent, D., Bonfond, B., Krupp, N., & Woch, J. (2008). Discontinuity in Jupiter's main auroral oval. *Journal of Geophysical Research*, 113(A1), A01215. <https://doi.org/10.1029/2007JA012610>
- Ranquist, D., Bagenal, F., Wilson, R., Hospodarsky, G., Ebert, R., Allegrini, F., et al. (2019). Survey of Jupiter's dawn magnetosheath using Juno. *Journal of Geophysical Research: Space Physics*, 124(11), 9106–9123. <https://doi.org/10.1029/2019JA027382>



- Ray, L. C., Achilleos, N. A., Vogt, M. F., & Yates, J. N. (2014). Local time variations in Jupiter's magnetosphere-ionosphere coupling system. *Journal of Geophysical Research: Space Physics*, *119*(6), 4740–4751. <https://doi.org/10.1002/2014JA019941>
- Sarkango, Y., Jia, X., & Toth, G. (2019). Global MHD simulations of the response of Jupiter's magnetosphere and ionosphere to changes in the solar wind and IMF. *Journal of Geophysical Research: Space Physics*, *124*(7), 5317–5341. <https://doi.org/10.1029/2019ja026787>
- Saur, J. (2004). Turbulent heating of Jupiter's middle magnetosphere. *The Astrophysical Journal Letters*, *602*(2), L137–L140. <https://doi.org/10.1086/382588>
- Saur, J., Janser, S., Schreiner, A., Clark, G., Mauk, B. H., Kollmann, P., et al. (2018). Wave-particle interaction of Alfvén waves in Jupiter's magnetosphere: Auroral and magnetospheric particle acceleration. *Journal of Geophysical Research: Space Physics*, *123*(11), 9560–9573. <https://doi.org/10.1029/2018JA025948>
- Scarf, F. L., Gurnett, D. A., & Kurth, W. S. (1979). Jupiter plasma wave observations: An initial Voyager 1 overview. *Science*, *204*(4396), 991–995. <https://doi.org/10.1126/science.204.4396.991>
- Sinclair, J., Orton, G., Fernandes, J., Kasaba, Y., Sato, T., Fujiyoshi, T., et al. (2019). A brightening of Jupiter's auroral 7.8- $\mu\text{m}$  CH 4 emission during a solar-wind compression. *Nature Astronomy*, *1*(7), 607–613. <https://doi.org/10.1038/s41550-019-0743-x>
- Southwood, D., & Kivelson, M. (2001). A new perspective concerning the influence of the solar wind on the Jovian magnetosphere. *Journal of Geophysical Research*, *106*(A4), 6123–6130. <https://doi.org/10.1029/2000JA000236>
- Stallard, T. S., Masters, A., Miller, S., Melin, H., Bunce, E. J., Arridge, C. S., et al. (2012). Saturn's auroral/polar H3+ infrared emission: The effect of solar wind compression. *Journal of Geophysical Research*, *117*(A12), A12302. <https://doi.org/10.1029/2012JA018201>
- Tao, C., Kataoka, R., Fukunishi, H., Takahashi, Y., & Yokoyama, T. (2005). Magnetic field variations in the Jovian magnetotail induced by solar wind dynamic pressure enhancements. *Journal of Geophysical Research*, *110*(A11), A11208. <https://doi.org/10.1029/2004JA010959>
- Vasyliunas, V. (1983). Plasma distribution and flow. *Physics of the Jovian magnetosphere*, *1*, 395–453. <https://doi.org/10.1017/CBO9780511564574.013>
- Vogt, M. F., Bunce, E. J., Kivelson, M. G., Khurana, K. K., Walker, R. J., Radioti, A., et al. (2015). Magnetosphere-ionosphere mapping at Jupiter: Quantifying the effects of using different internal field models. *Journal of Geophysical Research: Space Physics*, *120*(4), 2584–2599. <https://doi.org/10.1002/2014JA020729>
- Vogt, M. F., Gyalay, S., Kronberg, E. A., Bunce, E. J., Kurth, W. S., Zieger, B., & Tao, C. (2019). Solar wind interaction with Jupiter's magnetosphere: A statistical study of Galileo in situ data and modeled upstream solar wind conditions. *Journal of Geophysical Research: Space Physics*, *124*(12), 10170–10199. <https://doi.org/10.1029/2019JA026950>
- Vogt, M. F., Kivelson, M. G., Khurana, K. K., Walker, R. J., Bonfond, B., Grodent, D., & Radioti, A. (2011). Improved mapping of Jupiter's auroral features to magnetospheric sources. *Journal of Geophysical Research*, *116*(A3), A03220. <https://doi.org/10.1029/2010JA016148>
- Waite, J., Jr., Gladstone, G. R., Lewis, W. S., Goldstein, R., McComas, D. J., Riley, P., et al. (2001). An auroral flare at Jupiter. *Nature*, *410*(6830), 787–789. <https://doi.org/10.1038/35071018>
- Yao, Z., Bonfond, B., Clark, G., Grodent, D., Dunn, W., Vogt, M., et al. (2020). Reconnection and dipolarization driven auroral dawn storms and injections. *Journal of Geophysical Research: Space Physics*, *125*(8), e2019JA027663. <https://doi.org/10.1029/2019JA027663>
- Yao, Z., Grodent, D., Kurth, W. S., Clark, G., Mauk, B. H., Kimura, T., et al. (2019). On the relation between Jovian aurorae and the loading/unloading of the magnetic flux: Simultaneous measurements from Juno, HST and Hisaki. *Geophysical Research Letters*, *46*(21), 11632–11641. <https://doi.org/10.1029/2019GL084201>
- Zarka, P., & Genova, F. (1983). Low-frequency Jovian emission and solar wind magnetic sector structure. *Nature*, *306*(5945), 767–768. <https://doi.org/10.1038/306767a0>